Photothermally Triggered Cytosolic Drug Delivery *via* Endosome Disruption Using a Functionalized Reduced Graphene Oxide

Hyunwoo Kim,[†,‡] Duhwan Lee,[†,‡] Jinhwan Kim,[†,‡] Tae-il Kim,[§,*] and Won Jong Kim[†,‡,*]

[†]Center for Self-assembly and Complexity, Institute for Basic Science (IBS), Pohang, 790-784, Korea, [‡]Department of Chemistry Polymer Research Institute, Pohang University of Science and Technology (POSTECH), Pohang, 790-784, Korea, and [§]Department of Biosystems and Biomaterials Science and Engineering, College of Agriculture and Life Sciences, Seoul National University, Seoul 151-921, Korea

ABSTRACT Graphene oxide has unique physiochemical properties, showing great potential in biomedical applications. In the present work, functionalized reduced graphene oxide (PEG-BPEI-rGO) has been developed as a nanotemplate for photothermally triggered cytosolic drug delivery by inducing endosomal disruption and subsequent drug release. PEG-BPEI-rGO has the ability to load a greater amount of doxorubicin (DOX) than unreduced PEG-BPEI-GO *via* $\pi-\pi$ and hydrophobic interactions, showing high water stability. Loaded DOX could be efficiently released by glutathione (GSH) and the photothermal effect of irradiated near IR (NIR) in test tubes as well as in cells. Importantly, PEG-BPEI-rGO/DOX complex was found to escape from endosomes after cellular uptake by photothermally induced endosomal disruption and the proton sponge effect, followed by GSH-induced DOX release into the cytosol. Finally, it was concluded that a greater cancer cell death efficacy was observed in PEG-BPEI-rGO/DOX complex-treated cells with NIR irradiation than those with no irradiation. This study demonstrated the development of the potential of a PEG-BPEI-rGO nanocarrier by photothermally triggered cytosolic drug delivery *via* endosomal disruption.

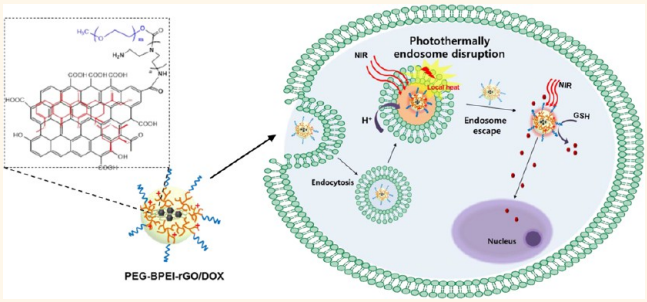

KEYWORDS: functionalized reduced graphene oxide · photothermal effect · near infrared stimuli-responsive · controlled drug delivery · endosome disruption

The development of external stimuli-triggered spatially and temporally controlled drug delivery carriers has received tremendous attention in recent years. These carriers have shown significant potential in targeted drug delivery through effective drug accumulation at target regions.[1,2] External stimuli, exploited for such applications, include light,[3,4] temperature,[5] magnetic field,[6] and ultrasound.[7,8] Among all stimuli, light provides a great opportunity to deliver a drug at the desired area in time, which is considered a key tool to amplify drug efficacy in cancer treatment with minimum adverse effects. Especially, near-infrared (NIR) light has recently been attracting attention and has proven to be a promising tool for both *in vivo* imaging and photothermal therapy. A key advantage of using light in the NIR window (650−900 nm), confined from the low end of the absorbance regions by hemoglobin to the high end of the absorbance regions by water, is the minimal absorbance by skin and tissue, thus providing deep tissue penetration.[9]

Recently, there is a tremendous interest in developing cooperative systems to control drug effects *via* NIR irradiation.[10,11] Synergy between drugs and NIR irradiation has been demonstrated through the addition of NIR-mediated photothermal agents, such as gold or carbon nanomaterials. Among such applications, NIR-responsive nanocarrier systems are still reported and strongly demanded. For example, Xia and co-workers have explored a gold nanocage covered by a temperature-responsive polymer[12] and phase change materials[13] for controlled release using NIR light. Some other groups proposed NIR-triggered oligonucleotide-gated

* Address correspondence to seal1004@snu.ac.kr, wjkim@postech.ac.kr.

Received for review March 31, 2013 and accepted July 7, 2013.

Published online July 07, 2013
10.1021/nn403096s

gold and mesoporous nanoparticle composites.[14] These nanomaterials, exhibiting photothermal effects, also could trigger disruption of the endo/lysosomal membranes by photoinduced local heat generation.[15,16] Volk and co-workers have explored NIR-activated gold nanoparticles leading to endosome rupture and escape into the cytosol without affecting the cell viability.[17] These promising results have strongly backed up studies on photothermally triggered cytosolic delivery of drug-loaded nanomaterials.

For several years, carbon nanomaterials have shown extraordinary potential in the field of drug delivery because of their six-membered carbon ring structure, which can allow $\pi-\pi$ interactions and hydrophobic interactions with drugs having aromatic rings.[18−20] Many reports have investigated the potential of graphene oxide (GO) as a drug delivery carrier since 2008. The large surface area of GO provides an ultrahigh drug loading efficiency. Dai's group has first investigated drug loading and release on GO,[19] illustrating the high drug loading capacity of GO, also studied in other reports.[21,22] It is also reported that GO possesses a larger surface area and higher mass extinction coefficient than gold nanorods. Moreover, GO is more applicable to nanomedicine and electrical devices because of its lower cost than carbon nanotubes, though having a similar mass coefficient.[23]

Over and above the delivery of small drug molecules, our group showed that functionalized GO sheets are capable of gene transfection in our previous work.[24,25] BPEI-conjugated GO (BPEI-GO) showed high gene delivery efficiency and high cell viability. In addition, Zhang's group has reported sequential delivery of siRNA and anticancer drugs into cancer cells.[26] Furthermore, GO-based nanomaterial has also received much attention as a new photothermally activated application using its strong NIR optical absorption ability such as *in vivo* photothermal therapy,[23,27,28] photothermal treatment of Alzheimer's disease,[29] photothermally enhanced drug delivery,[30] and photothermally responsive injectable hydrogels.[31] In particular, reduced GO (rGO) could be an improvement over GO with enhanced and modified optical properties, such as a photothermal effect,[23,32,33] and thus has engaged a lot of research interest.

In general, for drug delivery into the nucleus, a drug-loaded carrier should be able to escape from the endosome after endocytosis-mediated cellular uptake, followed by drug release from the carrier *via* drug−proteasome complex formation.[34] After endosomal escape by photothermally induced heat, the drug can also be released by glutathione (GSH) and NIR irradiation.[4] GSH, concentrated in the cytosol rather than the extracellular environment, is a unique internal stimulus for active drug and gene release inside cells.[35] According to a recent report, GSH could also trigger rapid drug release caused by the disruption of noncovalent hydrophobic interactions and $\pi-\pi$ stacking of the aromatic rings of GO sheets.[36]

In this study, we showed that functionalized rGO (PEG-BPEI-rGO) can be an excellent nanoplatform for photothermally controlled drug delivery. We developed a nanosized PEG-BPEI-rGO composite consisting of rGO sheets covalently conjugated with branched polyethylenimine (BPEI) and polyethylene glycol (PEG). The success of the functionalization of rGO has been established by ^{1}H NMR studies, Fourier transform infrared (FT-IR) spectroscopy, thermogravimetric analysis (TGA), and atomic force microscopy (AFM). The PEG-BPEI-rGO displays good colloidal stability and remains stable as a dispersion after loading with doxorubicin (DOX) *via* $\pi-\pi$ stacking and hydrophobic interactions. Herein, we uncovered that the functionalized rGO could be a nanotemplate for a tailor-made anticancer drug delivery carrier by photothermally controlled drug release *via* endosomal disruption, finally inducing higher cancer cell death.

RESULTS AND DISCUSSION

Synthesis and Characterization of PEG-BPEI-rGO. In our previous work, we reported the synthesis of BPEI-conjugated GO (BPEI-GO), consisting of GO and low molecular weight BPEI (LMW BPEI). In the present work, for an improved system, GO has been reduced for enhanced photothermal effect and PEGylation for increased colloidal stability, resulting in the synthesis of PEG-BPEI-rGO. In brief, BPEI 1.8K (M_w: 1.8 kDa) was covalently conjugated with the carboxylic acid group of GO using EDC/NHS chemistry, and the resulting BPEI-GO has been reduced by hydrazine monohydrate (0.05 v/v %) for 15 min at 80 °C followed by PEGylation through the CDI coupling reaction (Scheme 1).

The composition of GO in PEG-BPEI-rGO was analyzed by TGA and ^{1}H NMR. As shown in Figure S1a, GO is thermally unstable and starts to lose mass upon heating even below 100 °C, which was derived from the vaporization of stored water in its π-stacked structure. The major mass loss appeared close to 180 °C, which was ascribed to the pyrolysis of oxygen groups. TGA data for PEG-BPEI-rGO showed a 92.5% weight loss at 600 °C, whereas GO and pristine PEG-BPEI had weight losses of 75% and 99.5%, respectively. Therefore, we could calculate that the composite contains about 10 wt % GO in the PEG-BPEI-rGO. The conjugation ratio of PEG to BPEI in PEG-BPEI-rGO was found to be 0.8 (molar ratio), as determined by ^{1}H NMR analysis (Figure S1b). The successful BPEI conjugation to the carboxylic acid group of GO and chemical reduction of PEG-BPEI-rGO were estimated by FT-IR spectroscopy (Figure S2a).[37] The band at 1050 cm^{-1}, indicating the presence of C−O stretching in GO, was diminished in reduced PEG-BPEI-rGO, proving the reduction of GO. Raman analysis also corroborated proof of GO reduction. A change of value in the intensity ratio between

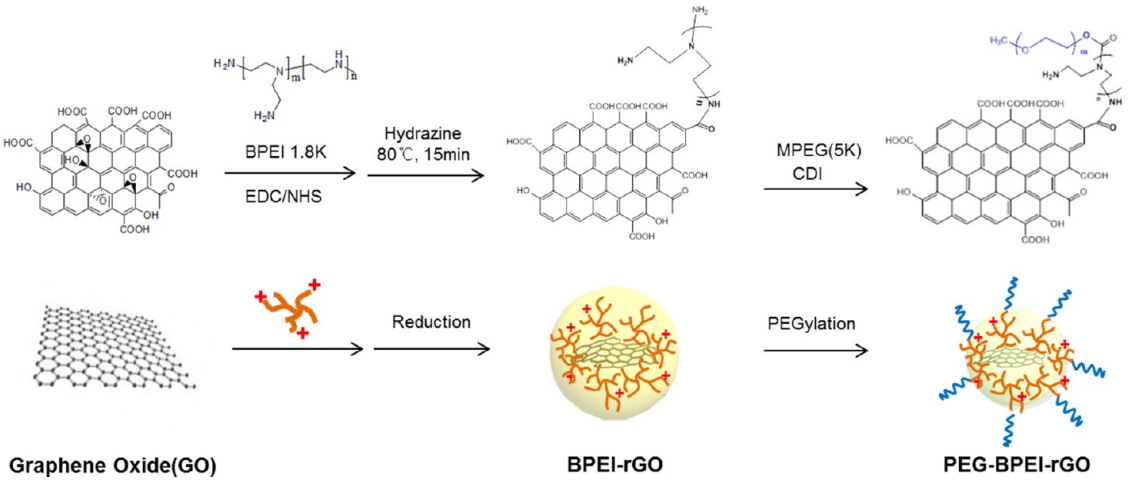

Scheme 1. Schematic illustration of the preparation of PEG-BPEI-rGO.

the D and G peaks from 0.97 to 1.13 was observed after BPEI conjugation and reduction (Figure S2b).[38] It has also been reported that carbon nanomaterials, such as carbon nanotubes,[39] graphene,[28] and GO, are shown to generate heat under NIR irradiation, and the reduced form of GO has a more effective photothermal property.[23] The excellent optical absorbance of nanomaterials containing GO of around 800 nm leads to its effective application in biomedicine because of its minimal absorbance of water molecules and tissue components in this region. To examine the optical property of GO, PEG-BPEI-GO, and PEG-BPEI-rGO, UV/vis absorbance spectroscopy data hasve been collected (Figure S2c). All the GO-based materials exhibit UV/vis absorbance over a wide range of wavelengths, and the absorbance of PEG-BPEI-rGO was found to be higher than that of the unreduced form. The difference in absorbance has been accounted for by the reduction of PEG-BPEI-GO with hydrazine monohydrate, leading to the restoration of the conjugated aromatic clusters.

Characterization of Drug-Loaded PEG-BPEI-rGO. As we mentioned above, many research groups investigated the potential of GO as a drug delivery carrier because of its large surface area for an ultrahigh drug loading efficiency. Hence, PEG-BPEI-rGO with two aromatic sheets is capable of adsorbing most of the aromatic anticancer drugs through its $\pi-\pi$ stacking and hydrophobic interactions, as illustrated in Figure 1a. Doxorubicin, used here as an anticancer drug, is an effective drug against various cancer cell lines. DOX has been noncovalently loaded onto water-dispersible PEG-BPEI-rGO by simple mixing for 12 h. After removal of free DOX by dialysis and centrifuge filtration, the observation of the deep red appearance of the PEG-BPEI-rGO dispersion by the unaided eye indirectly proves the DOX loading on PEG-BPEI-rGO. As expected, the PEGylated PEG-BPEI-rGO as well as DOX-loaded PEG-BPEI-rGO suspension was stable, unlike unmodified GO/DOX and non-PEGylated BPEI-rGO (Figure S3). The amount of loaded DOX on PEG-BPEI-rGO was quantified using UV/vis absorbance, with a distinguished DOX peak appearing at around 520 nm over the background of the carrier (Figure 1b). The amount of DOX loaded onto PEG-BPEI-rGO was estimated by measuring the absorbance at 520 nm for DOX, after subtracting the absorbance from that for the PEG-BPEI-rGO. It was found that the drug loading capacity for PEG-BPEI-rGO was remarkably higher than that of the unreduced form, PEG-BPEI-GO (about 100% for PEG-BPEI-rGO and only about 10% for PEG-BPEI-GO, Figure 1c). The difference in the loading capacity of these two carriers could be attributed to the large number of aromatic ring structures obtained upon reduction, and that results in the difference in the $\pi-\pi$ stacking and hydrophobic interactions with DOX. Subsequently, the interaction between PEG-BPEI-rGO and DOX was confirmed by measurement of fluorescence change. The loading process results in fluorescence quenching of DOX due to the photoinduced electron-transfer effect;[40] however interestingly, fluorescence could be recovered by addition of ethanol. The presence of ethanol is destructive to the noncovalent interaction between DOX and PEG-BPEI-rGO, meaning desorption of DOX from PEG-BPEI-rGO and, thus resulting in fluorescence recovery (Figure 1d). As shown in Figure 1e, the DOX loading onto PEG-BPEI-rGO exhibited excellent stability in physiological solutions such as saline and cell medium over 48 h. As we mentioned in Figure 1b, PEG-BPEI-rGO has a higher NIR absorbance than GO and PEG-BPEI-GO because of restoration of fused aromatic clusters upon reduction. GO-containing nanomaterials can transfer absorbed energy to thermal energy, and thus we investigated the heat generation upon NIR laser irradiation (808 nm, 6 W/cm^2) of the various solutions containing PEG-BPEI-rGO/DOX, PEG-BPEI-rGO, PEG-BPEI-GO, GO, and a control without GO, as shown in Figure 1f.

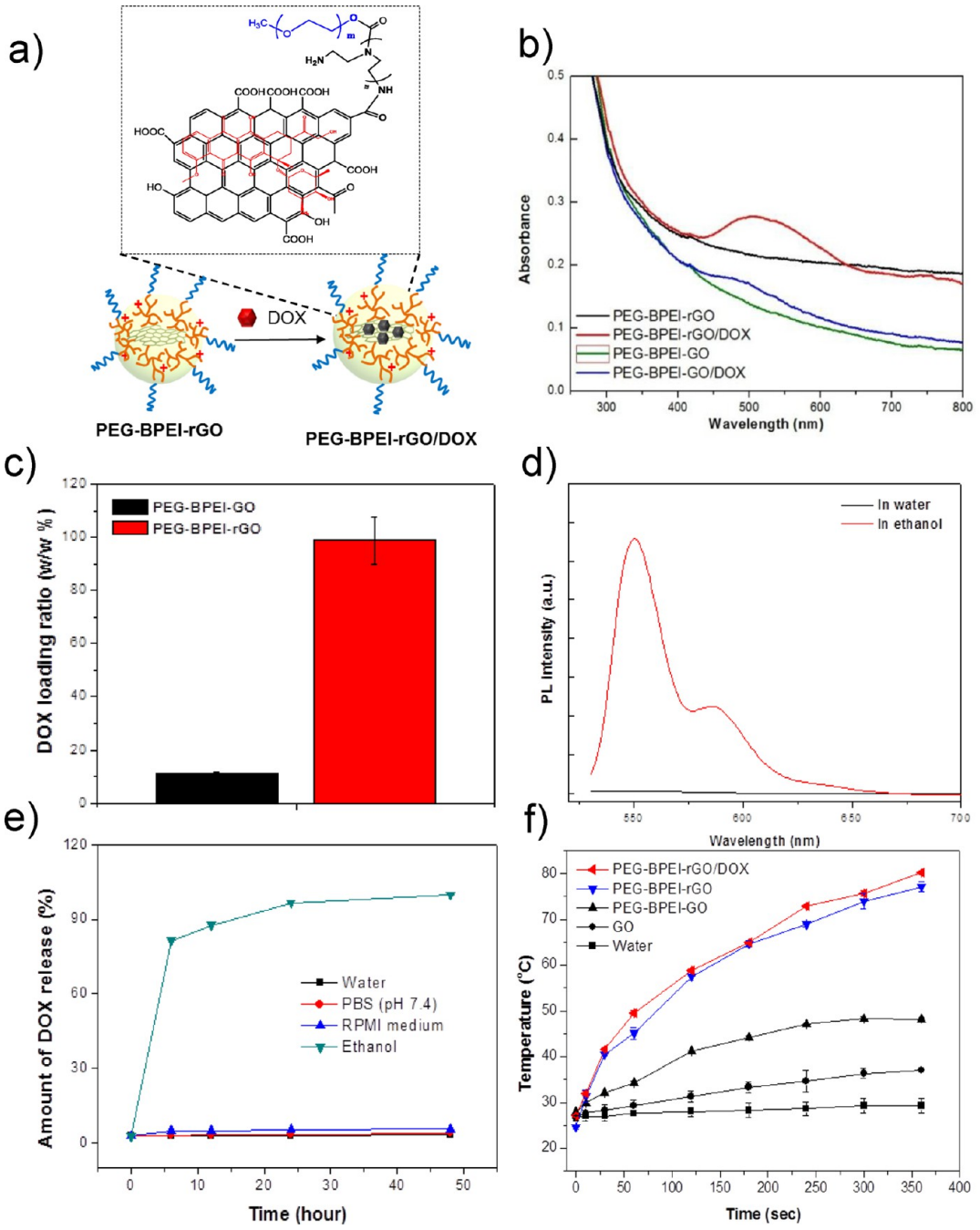

Figure 1. (a) Schematic drawings of DOX $\pi-\pi$ stacking onto a rGO prefunctionalized by BPEI conjugation and PEGylation. (b) UV/vis/NIR absorbance spectra of solutions of PEG-BPEI-rGO, PEG-BPEI-rGO/DOX, PEG-BPEI-GO, and PEG-BPEI-GO/DOX. (c) Comparison of drug loading capacity of PEG-BPEI-rGO and PEG-BPEI-GO. (d) Fluorescence spectra of DOX before and after adsorption on PEG-BPEI-rGO in water and 99% ethanol. (e) Amount of DOX release from PEG-BPEI-rGO incubated in water, PBS, RPMI medium, and ethanol. (f) Measurement of temperature of GO, PEG-BPEI-rGO, and PEG-BPEI-rGO/DOX (containing 0.05 mg/mL GO) under NIR irradiation (808 nm, 6 W/cm^2).

As expected, control water had no response to NIR irradiation, whereas solutions containing PEG-BPEI-rGO/DOX, PEG-BPEI-rGO, PEG-BPEI-GO, and GO showed different GO-mediated heat generation. Moreover, both reduced PEG-BPEI-rGO and PEG-BPEI-rGO/DOX showed a higher temperature increase (~40 °C) as compared to unreduced PEG-BPEI-GO and GO possibly because of effective restoration of the π conjugation by chemical reduction. Therefore, it might be suggested that the energy absorbed by the photoactivated GO-based nanomaterials can be quickly transferred to molecular vibration energies and finally converted into thermal energy.

The effect of DOX loading on the size and morphology of GO and PEG-BPEI-rGO has also been investigated by AFM (Figure 2). The size and thickness

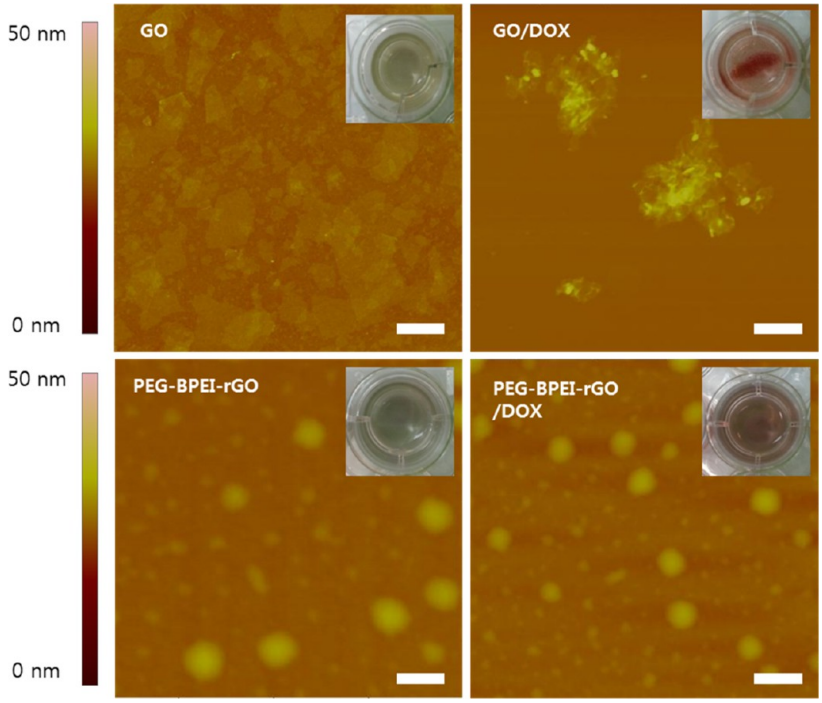

Figure 2. AFM images of GO, PEG-BPEI-rGO, GO/DOX aggregates, and PEG-BPEI-rGO/DOX. A droplet of GO and PEG-BPEI-rGO dispersion was cast onto a freshly prepared silicon oxide wafer (p-type), followed by drying at 80 °C. The scale bar is 250 nm.

of the unmodified GO were about 500−700 nm and 0.6−1.3 nm, respectively, as shown in the AFM image. Interestingly, the PEG-BPEI-rGO was found to have a round shape, a reduced diameter of 100−200 nm, and an increased thickness of about 15 nm compared to unmodified GO. This could be attributed to the folding and re-forming of the GO sheet during the EDC/NHS-mediated reaction and sonication process, and the round shape of PEG-BPEI-rGO could be ascribed to the PEGylation surrounding BPEI-rGO.[41] It was observed that the GO and DOX complex formed aggregates as shown in the AFM images. In contrast, PEG-BPEI-rGO/DOX exhibited no significant change of diameter and thickness in comparison with PEG-BPEI-rGO without DOX loading. This result implies that the functionalized rGO is a more stable drug carrier platform and thus has more potential as a drug carrier than pristine GO.

Stimuli-Triggered Drug Release. Here, we focused on extra- and intracellular stimuli-responsive release of loaded drug molecules such as NIR irradiation, GSH concentration, and acidic condition. Figure 3a and b show a recovered DOX fluorescence intensity released from PEG-BPEI-rGO, when a fixed concentration of PEG-BPEI-rGO/DOX was incubated with an increasing NIR irradiation time (0−3 h) and GSH concentration (0−10 mM). It was observed that both GSH and NIR irradiation accelerated drug release. A comparison of drug releasing ability of stimuli is illustrated in Figure 3c, showing a drug release upon NIR irradiation, GSH, and acidic conditions of about 15%, 37%, and 10% for 180 min, respectively (Figure 3c), while DOX release was increased by ∼45% upon application of multiple stimuli to the PEG-BPEI-rGO/DOX solution (Figure 3d). The drug release acceleration upon NIR triggering is most likely associated with changing of the binding energy between PEG-BPEI-rGO and DOX.[18,42] The drug release data showed a difference between samples in control (dark) condition and with NIR irradiation. This behavior can be attributed to a change of binding energy between PEG-BPEI-rGO and DOX by NIR-mediated heat generation, which is thus favorable for drug release. The GSH also could trigger rapid drug release caused by the disruption of non-covalent hydrophobic interactions and $\pi-\pi$ stacking of the aromatic regions of the GO sheets.[36] The low pH also slightly accelerates the release of DOX loaded on PEG-BPEI-rGO, as evident by a previous report.[43] At low pH, DOX becomes more hydrophilic due to the protonation of its NH_2 group and thus a greater amount of DOX could be released from the PEG-BPEI-rGO. It is expected that drug release in cells could be induced by a combination of multiple stimuli such as acidic pH, the presence of GSH, and NIR irradiation.

Photothermally Triggered Endosome Disruption. As described above, the photothermal effect on PEG-BPEI-rGO can trigger the disruption of the endo/lysosomal membranes after cellular uptake by photoinduced local heat generation. To explore the potential of PEG-BPEI-rGO as a photothermally controlled drug carrier, we first studied the cellular uptake of the FITC-labeled PEG-BPEI-rGO in dark condition and under NIR irradiation by confocal fluorescence imaging

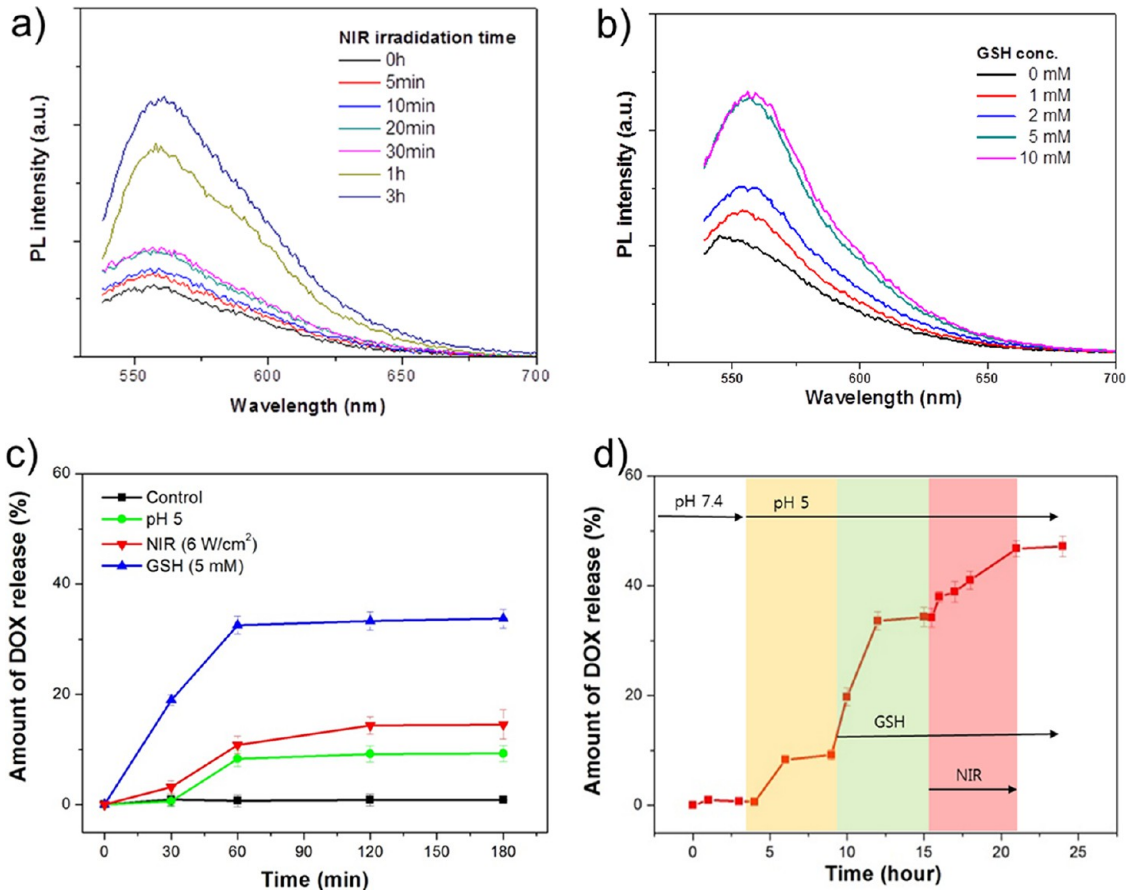

Figure 3. Fluorescence spectra of the PEG-BPEI-rGO/DOX complex with increasing NIR irradiation time (a) and GSH concentration (b). (c) Plot of the stimuli-induced DOX release from PEG-BPEI-rGO at acidic condition (pH 5), with NIR irradiation (6 W/cm^2), and with GSH (5 mM) over 3 h. (d) Sequential multistimuli-responsive DOX release profile from PEG-BPEI-rGO/DOX complex under acidic condition (pH 5), with GSH (5 mM), and with NIR irradiation (6 W/cm^2).

and flow cytometric analysis. It was evident from the experimental data that the green fluorescence intensity in the dark was similar to that under NIR irradiation qualitatively (confocal image) and quantitatively (flow cytometry), meaning that cellular uptake of the PEG-BPEI-rGO was not significantly affected by NIR irradiation compared to cells incubated in the dark condition (Figure S5). Consequently, NIR itself did not have any effect on the cellular uptake of carriers. Second, we investigated the intracellular distribution of PEG-BPEI-rGO after cellular uptake. To trace the intracellular distribution, FITC-labeled PEG-BPEI-rGO has been monitored by confocal laser microscopy (Figure 4). Without NIR irradiation, FITC-labeled PEG-BPEI-rGO (green) was localized in endo/lysosomal compartments, as observed by staining with LysoTracker (red), substantiating the cellular uptake of carrier by endocytosis and entrapment within the endosome.[44] In contrast, after NIR irradiation (808 nm laser, 30 min) in the FITC-labeled PEG-BPEI-rGO-treated cells, the green fluorescence from PEG-BPEI-rGO was observed as more diffused spots in the cytosol, which is clearly distinguishable from the red fluorescence emanating from LysoTracker, implying endosomal escape of the PEG-BPEI-rGO carrier. Without NIR irradiation, only a few green fluorescent spots were found outside the endo/lysosomes over the same time period. These observations indicate that PEG-BPEI-rGO successfully escaped from the endosome by NIR irradiation before lysosomal degradation, which subsequently could induce high drug efficacy by GSH-mediated drug release in the cytosol.

Extra- and Intracellular Stimuli-Triggered Drug Release in Cells. As described in Scheme 2, NIR irradiation could induce photothermal endosomal disruption in cells after treatement with PEG-BPEI-rGO. Therefore, we examined the DOX release from the PEG-BPEI-rGO/DOX complex after cellular uptake upon NIR irradiation *in vitro*. PC-3 cells were incubated with PEG-BPEI-rGO/DOX for 4 h, and excess PEG-BPEI-rGO was completely washed out, followed by NIR irradiation for 0, 10, 20, and 30 min. The fluorescence of DOX on PEG-BPEI-rGO was initially quenched by the photoinduced electron transfer effect. Upon NIR irradiation, the photothermal heating caused a change in binding energy between PEG-BPEI-rGO and DOX, leading to desorption of DOX from the carrier and diffusion of DOX into the cytosol of the cells. The amount of released DOX, reflected by the

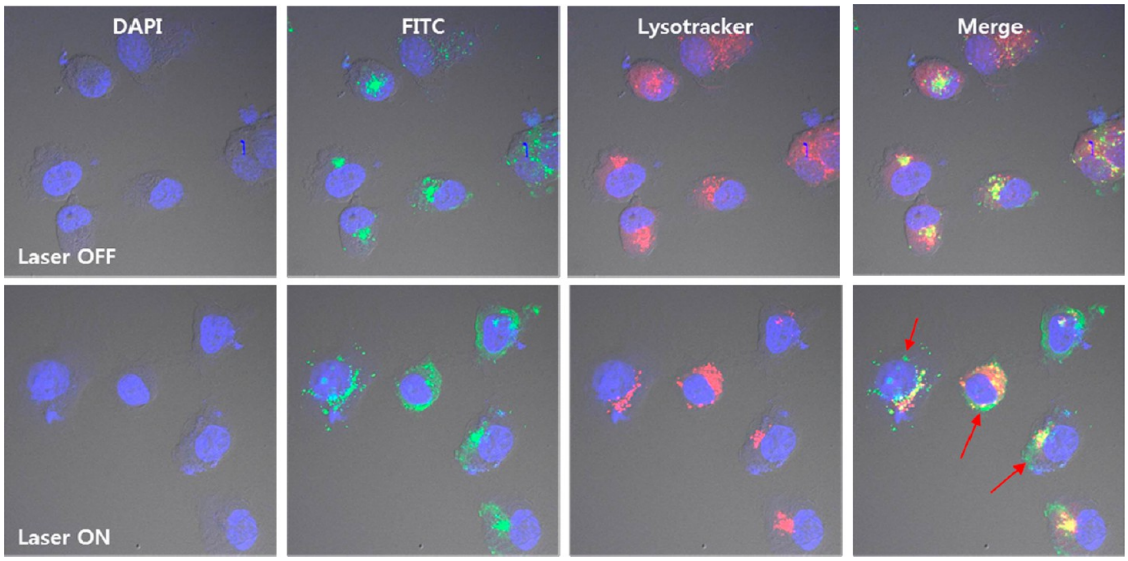

Figure 4. Confocal fluorescence microscopic images of PC-3 cells treated with PEG-BPEI-rGO/DOX complexes in the dark (top) or under NIR irradiation (bottom). Nuclei were stained with DAPI (blue), PEG-BPEI-rGO was labeled with FITC (green), and endo/lysosomes were stained with LysoTracker (red).

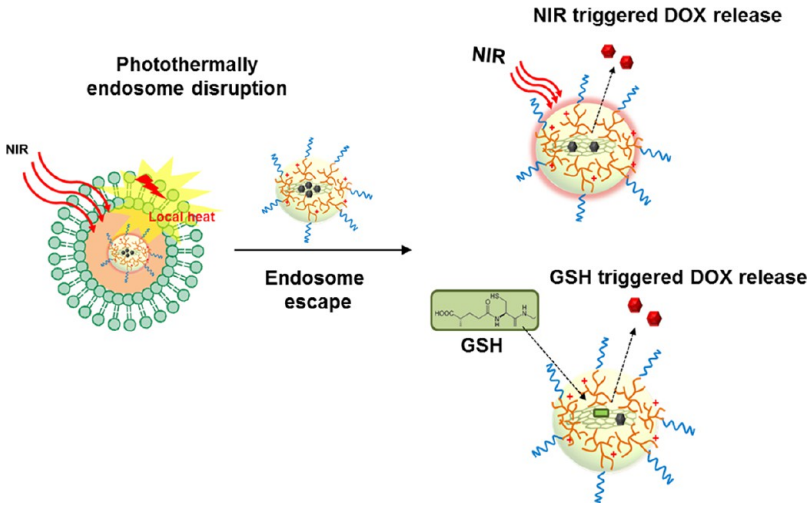

Scheme 2. Schematic illustration of the mechanism of cytosolic drug release by NIR and GSH after photothermally induced endosome disruption.

fluorescence of the whole cell, was estimated by flow cytometric analysis (Figure 5a and b). Noticeably, a right shift of the fluorescence profile was also observed in the sample that was not NIR irradiated, attributable to unquenched background DOX fluorescence and the small number of DOX liberated from carriers by passive diffusion during the 4 h of incubation. Following 10 min of NIR irradiation, the fluorescence signal of the DOX was shifted to the right distinctly, indicating a significant release of drug into the cells, whereas longer NIR irradiation did not cause any further increase of DOX release into cells. In the control, cells were treated with free DOX without PEG-BPEI-rGO, followed by NIR irradiation, and it was observed that NIR irradiation did not accelerate the DOX release, although there was a slight passive diffusion of DOX into cells. Then, we studied the time-dependent release of DOX at different incubation times (3, 6, and 12 h) by confocal fluorescence imaging. Stronger red fluorescence of DOX was observed in NIR-irradiated cells than untreated control cells with increase in incubation time. This result can be explained by the drug-loaded carrier easily escaping under NIR irradiation by photothermally enhanced endosomal disruption, and the drug release from GO could be accelerated by interaction with GSH in the cytosol. Therefore, a long incubation time could extend the chances of interaction between the carrier and GSH, resulting in enhanced drug release (Figure 5c).

***In Vitro* Anticancer Effect by a Photothermally Controlled Drug Release System.** The evaluation of the therapeutic efficacy of DOX-loaded PEG-BPEI-rGO was carried out *in vitro* by quantifying the cell viability of PC-3 and

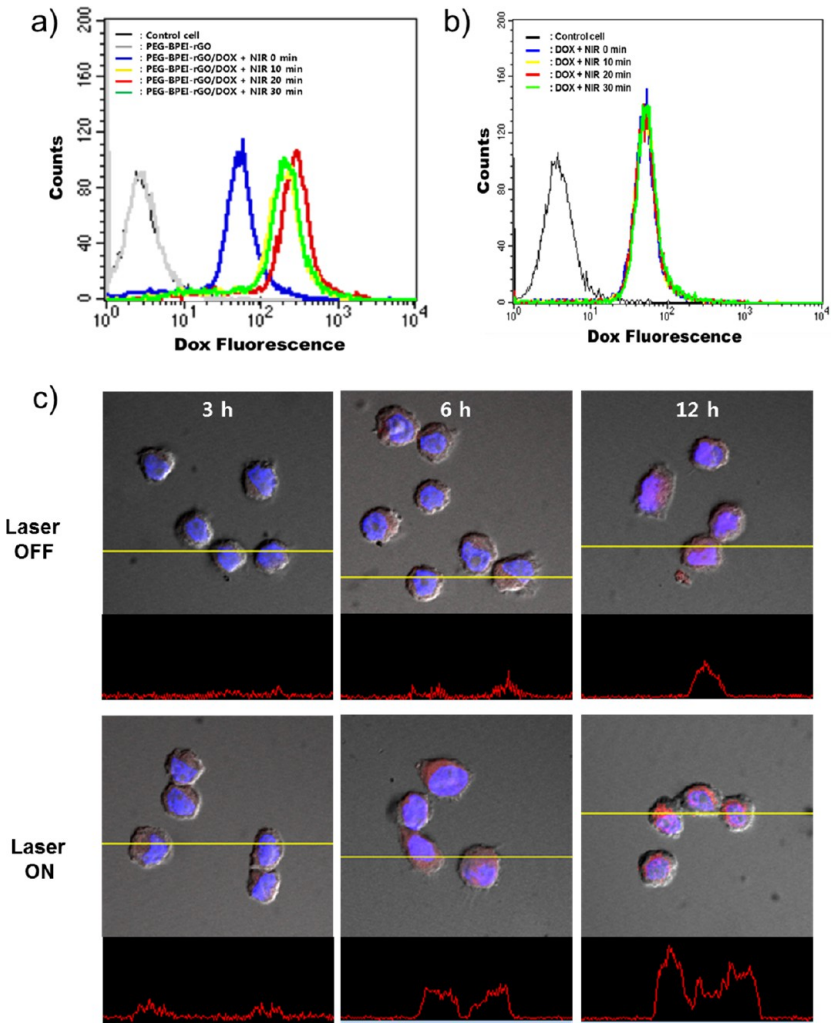

Figure 5. NIR-responsive DOX release from PEG-BPEI-rGO *in vitro*. Flow cytometry histogram profile of recovered DOX fluorescence from PEG-BPEI-rGO/DOX complexes (a) and free DOX fluorescence (b) in PC-3 cells upon different NIR irradiation times. (c) Confocal microscopic images in PC-3 cells treated with PEG-BPEI-rGO/DOX complexes in the dark (top) and under NIR irradiation (bottom) after various incubation times (3, 6, 12 h). Nuclei were stained with DAPI (blue), DOX has specific light emission (red).

HeLa cells using the MTT assay. The potential nonspecific toxicity of the carrier is always a great concern for nanomaterials used in biomedicine. Prior to evaluation of DOX-loaded PEG-BPEI-rGO, a cytotoxicity study of PEG-BPEI-rGO on PC-3 and HeLa cells was carried out as a function of the concentration of PEG-BPEI-rGO (0−400 μg/mL) under NIR irradiation (808 nm, 6 W/cm^2, 30 min). As shown in Figure 6a, cell viability remained above 90%, even above the PEG-BPEI-rGO concentration of 400 μg/mL in the dark and below the concentration of 100 μg/mL under NIR irradiation. This result revealed that the PEG-BPEI-rGO did not have any obvious toxic effect, and the NIR-induced photothermal effect of PEG-BPEI-rGO also did not affect cell viability below the concentration 100 μg/mL, which is the upper limit concentration of the anticancer experiments done in this study. To evaluate *in vitro* cytotoxicity of the free DOX and PEG-BPEI-rGO/DOX under NIR irradiation, PC-3 and HeLa cells were incubated with different concentrations of DOX for 48 h, where the PEG-BPEI-rGO/DOX has an equivalent DOX dosage to free DOX (Figure 6b and c). As expected, cell viability of PEG-PBEI-rGO/DOX-treated cells was about 20% decreased in the NIR irradiation condition as compared with the dark condition, which clearly shows the enhanced and controllable release of drug molecules from PEG-BPEI-rGO by the photothermal effect. In the case of free DOX, there was no significant difference of cell viability between NIR irradiation and dark condition. Interestingly, HeLa cells were found to be more susceptible to DOX than PC-3 cells, revealing cell line dependency of DOX. Overall drug-loaded PEG-BPEI-rGO showed lower cytotoxic effects than free DOX, as shown in Figure 6b and c. However, when incubated with drug-loaded PEG-BPEI-rGO, NIR irradiation caused a higher amount of cell death than nontreated cells, while there are no significant differences between the NIR laser on and off when incubated with free DOX.

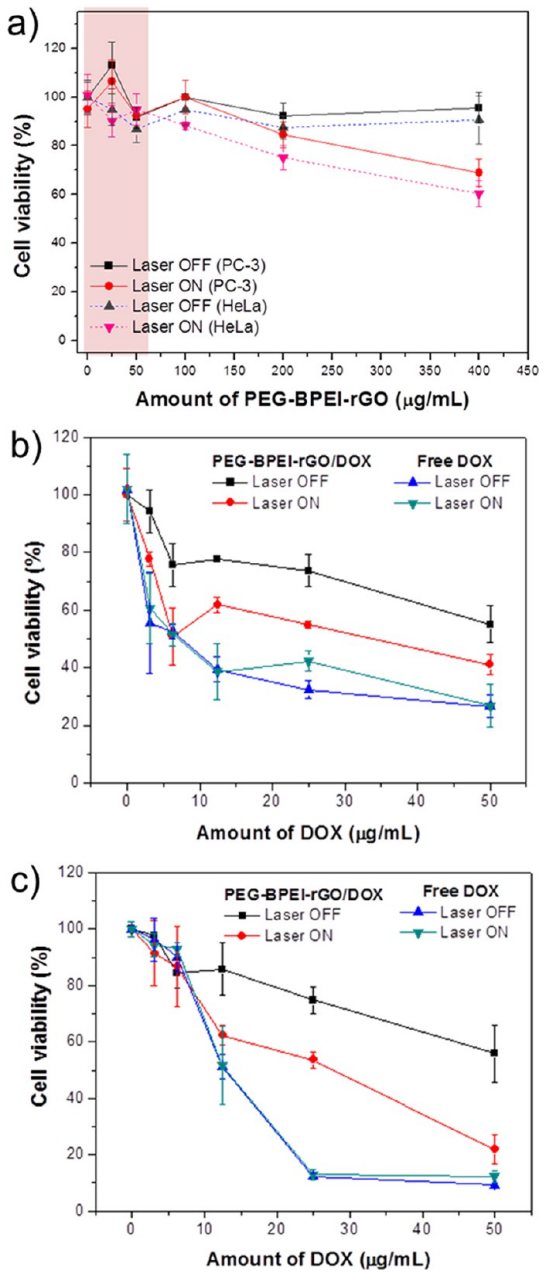

Figure 6. (a) MTT assay to assess the cell viability of PC-3 and HeLa cells incubated with various PEG-BPEI-rGO (0−400 μg/mL) concentrations in the dark or under NIR irradiation, and cell viability profile of PC-3 cells (b) and HeLa cells (c) treated with PEG-BPEI-rGO/DOX and free DOX with a various DOX (0−50 μg/mL) concentrations in the dark or under NIR irradiation.

The low cytotoxic effect observed in PEG-BPEI-rGO/DOX-treated cells could be attributed to delayed DOX release from PEG-BPEI-rGO and endocytosis-mediated cytosolic delivery, which is controlled to some extent by endosomal disruption. DOX was known to be an effective anticancer drug, but it has been difficult to maintain the balance between maximum safe concentration and minimum effective concentration after administration. Therefore, with consideration of the above results, although PEG-BPEI-rGO/DOX showed less cancer killing effect than free DOX, it can deliver drug molecules in a remotely and conveniently controllable way, and thus it is considered to be a very attractive nanotemplate for a drug carrier system. From the above results, it was revealed that photothermally induced endosomal disruption affects the PEG-BPEI-rGO/DOX-mediated cell toxicity. It is also known that endosomal disruption can be accelerated by BPEI *via* its proton sponge effect. Therefore, we investigated whether BPEI of the carrier will increase the drug effect by endosomal disruption. We measured the cell viability of PEG-BPEI-rGO/DOX-treated PC-3 cells with and without bafilomycin A1, which is known to inhibit the proton pump in endosomal membranes[45] (Figure S6). Cell viability without bafilomycin A1 was found to be lower than that with bafilomycin A1, supporting the fact that PEG-BPEI-rGO/DOX was partially released from the endosome because of the proton sponge effect of BPEI. Therefore, it is concluded that endocytosed PEG-PEI-rGO can escape from the endosome by photothermally induced endosome disruption of rGO as well as the proton sponge effect of BPEI.

CONCLUSION

Here, we developed a photothermally triggered drug delivery system based on a functionalized reduced graphene oxide nanotemplate. This PEG-BPEI-rGO showed high water stability and dramatically enhanced DOX loading efficiency in comparison with unreduced PEG-BPEI-GO due to the recovery of aromatic structures of GO. Photothermal endosome disruption and the resulting NIR-responsive release of loaded DOX from PEG-BPEI-rGO in combination with GSH-mediated drug release were confirmed with NIR irradiation. Importantly, it was found that the PEG-BPEI-rGO nanocarrier could escape the endosome by photothermally induced endosomal disruption of GO as well as theh proton sponge effect of BPEI, finally killing more cancer cells with NIR irradiation than without irradiation. This work demonstrates the potential and the drug delivery mechanism of PEG-BPEI-rGO for photothermally controllable drug delivery systems, which can be further applied to many other nanomedicine fields.

EXPERIMENTAL SECTION

Synthesis of PEG-BPEI-rGO. Previously we reported the synthesis of functionalized GO (BPEI-GO) consisting of GO and low molecular weight BPEI (LMW BPEI).[24] In brief, BPEI 1.8K was covalently conjugated to the carboxylic acid group of GO using EDC/NHS chemistry, EDC (54 mg, 0.4 mmol) and NHS (51 mg, 0.4 mmol) were added to the GO solution (0.5 mg/mL) in a vial, and TEA (100 μL) was added to a BPEI solution (400 mg) in

deionized water. Next, the BPEI solution was added to the GO solution, and the mixture was sonicated for 3 h and then stirred for 24 h at room temperature. The resulting BPEI-GO solution was dialyzed by a dialysis membrane (MWCO: 3.5 kDa) in deionized water for 2 days to remove the unreacted BPEI, TEA, and coupling reagents. The reducing process of BPEI-GO was conducted by treating with 0.05% v/v of hydrazine monohydrate (80%) followed by heating to 80 °C for 15 min. In order to enhance the colloidal stability of BPEI-rGO, methoxypolyethyleneglycol (MPEG, 5 K) was incorporated by CDI coupling. For the activation of MPEG, MPEG (0.2 mmol) and CDI (1 mmol) were dissolved in anhydrous DCM (5 mL) followed by the addition of CDI solution into the MPEG solution with stirring under a nitrogen atmosphere for 12 h at room temperature. Next, a small amount of deionized water (100 μL) was added into the solution to inactivate the unreacted CDI. After evaporation of the solvent using a rotary evaporator, the PEG product was precipitated with ice-cold diethyl ether and dried under vacuum. For PEG conjugation to BPEI-rGO, activated PEG (5 mmol) in deionized water was added to BPEI-rGO (5 mmol of BPEI in BPEI-rGO) in deionized water. After reaction for 12 h at room temperature with stirring, the final product (PEG-BPEI-rGO) was dialyzed by a dialysis membrane (MWCO: 10 kDa) against deionized water.

Characterization of PEG-BPEI-rGO. The conjugation ratios of MPEG to BPEI in PEG-BPEI-rGO were determined by ^{1}H NMR. The composition of GO in PEG-BPEI-rGO was analyzed by TGA (Seiko Instrument, Japan). The diameter and morphology of GO and PEG-BPEI-rGO were investigated by a tapping mode atomic force microscope (Nanoscope IIIa, Digital Instrument Inc., USA). A droplet of GO and PEG-BPEI-rGO dispersion (about 0.01 mg/mL) was cast onto a freshly prepared silicon oxide wafer (p-type), followed by drying at 80 °C. The chemical conjugation of BPEI to GO was confirmed by FT-IR spectroscopy (VERTEX70 FT-IR spectrophotometer, Bruker Optics, Germany) using a KBr pellet. The chemical reduction of PEG-BPEI-rGO was confirmed using a confocal Raman spectroscope (Alpha 300R, WITec, Germany), FT-IR spectroscopy, and UV/vis spectrophotometry (UV 2550, Shimadzu, Japan) (see the Supporting Information).

Characterization of Drug-Loaded PEG-BPEI-rGO. Loading of an anticancer drug on the PEG-BPEI-rGO was carried out by adding DOX (DMSO solution) to the PEG-BPEI-rGO dispersed solution with stirring at room temperature for 12 h. The unbound DOX molecules were then removed by dialyzing against distilled water for more than 24 h. PEG-BPEI-rGO was repeatedly washed out by filtration through a centrifugal filter (MWCO: 3 kDa) and centrifuged at 4000 rpm for 20 min. The loading capacity of DOX in the carrier was evaluated from the absorbance at 520 nm, deducting the absorbance of the carrier. For the comparison of stability of unmodified GO and functionalized GO, we observed the stability change before and after DOX loading through AFM and the unaided eye, respectively. The stable drug loading ability onto PEG-BPEI-rGO was estimated at various conditions: DOX-loaded PEG-BPEI-rGO was incubated in water, PBS (pH 7.4), RPMI medium, and ethanol. The PEG-BPEI-rGO with or without DOX, PEG-BPEI-GO, and GO solution (0.05 mg/L) were diluted with 1 mL of deionized water and irradiated using a 808 nm laser (diode laser, JENOPTIK unique-mode GmbH, Germany) on 0.9 cm spot diameters at 6 W/cm^2. During the NIR irradiation, the temperature of the solution was measured by a thermocouple linked to a digital thermometer (Lutron thermometer TM-917, Taiwan) every 20 s for 6 min.

Multiple Stimuli-Triggered Drug Release. The amount of DOX released under various conditions was estimated by measurement of fluorescence at 550 nm. The solution with DOX-loaded PEG-BPEI-rGO (0.01 mg/mL) was incubated under NIR irradiation (808 nm laser at 6 W/cm^2), with a range of GSH concentrations (5 mM), and under acidic condition (pH 5) for predetermined times (0−3 h). The amount of DOX release was evaluated by measurement of the DOX fluorescence.

Flow Cytometric Analysis. PC-3 cells were seeded in 24-well culture plates (6×10^4 cells/well, $n = 3$) with 500 μL of RPMI medium and incubated in a humidified 5% CO_2 atmosphere at 37 °C for 24 h. Then, DOX-loaded PEG-BPEI-rGO complexes were incubated with the cells for 4 h, followed by washing three times. The cells were irradiated with an 808 nm laser at 6 W/cm^2 for 30 min. Then, the cells were incubated with 200 μL of 0.25% trypsin/EDTA for 10 min at 37 °C for detachment. The harvested cells were centrifuged, and the supernatant was removed. Cell suspensions were kept in 200 μL of 4% paraformaldehyde solution for 15 min of fixation and centrifuged again to remove the solution. DPBS solution (400 μL) supplemented with 2% FBS was added for measurement of fluorescence inside the cells (1×10^4) for each sample. The cells were analyzed with a FACS Calibur (Becton Dickinson) and BD Cell Quest software (Becton Dickinson), by following the procedure provided from the manufacturer.

Confocal Laser Scanning Microscope (CLSM) Study. PC-3 cells were seeded at a density of 1×10^4 cells/well in a 12-well plate over glass coverslips. Cells were incubated with samples/DOX complexes for 4 h at 37 °C. Then, cells were immediately irradiated by the 808 nm laser at a power density of 6 W/cm^2 for 30 min in 500 μL of fresh media containing 10% FBS and were incubated in 5 μM LysoTracker for 5 min. After quenching the cellular uptake by adding cold DPBS, cells were washed twice with cold DPBS and fixed with 4% paraformaldehyde for 30 min at room temperature. Cells on coverslips were mounted in Vectashield antifade mounting medium with DAPI (Vector Laboratories), observed with CLSM, and analyzed with OLYMPUS FLUOVIEW ver. 1.5 Viewer software.

Photothermally Controlled Drug Effect by NIR Irradiation *in Vitro*. The cytotoxicity of free DOX and PEG-BPEI-rGO with/without DOX was evaluated by the MTT assay. Cells were seeded onto 96-well plates at a density of 1×10^4 cells/well and incubated for 24 h. Samples were treated with the cells for 4 h in 100 μL of serum-free media. Then, cells were immediately irradiated by the 808 nm laser at a power density of 6 W/cm^2 for 30 min in 200 μL of fresh media containing 10% FBS followed by further incubation for 44 h. Cell media was replaced with 200 μL of fresh media and 20 μL of MTT solution (5 mg/mL) and incubated for another 4 h. The media was then removed, and 150 μL of DMSO was added into the wells to dissolve the purple formazan crystals formed by proliferating cells. An aliquot of 100 μL was taken from each well and transferred into a fresh 96-well plate. The absorbance was measured at 570 nm using a microplate spectrofluorometer (VICTOR3 V multilabel counter). The relative percentages of the control cells (nontreated), which were not treated with samples, were used to represent 100% cell viability.

Conflict of Interest: The authors declare no competing financial interest.

Acknowledgment. This work was supported by the Research Center Program of IBS (Institute for Basic Science) in Korea (CA1203-02).

Supporting Information Available: Detailed materials and reagents; estimation of composition of PEG-BPEI-rGO (TGA, ^{1}H NMR); determination of reduction of PEG-BPEI-rGO (FT-IR, Raman, UV/vis); evaluation of colloidal stability after DOX loading; observation of multiple stimuli-responsive DOX release profile; observation of cellular uptake of PEG-BPEI-rGO (confocal microscope, flow cytometry); study of proton sponge effect of PEG-BPEI-rGO; estimation of temperature-dependent DOX release and drug effect. This material is available free of charge *via* the Internet at http://pubs.acs.org.

REFERENCES AND NOTES

1. Fleige, E.; Quadir, M. A.; Haag, R. Stimuli-Responsive Polymeric Nanocarriers for the Controlled Transport of Active Compounds: Concepts and Applications. *Adv. Drug Delivery Rev.* **2012**, *64*, 866–884.
2. Timko, B. P.; Dvir, T.; Kohane, D. S. Remotely Triggerable Drug Delivery Systems. *Adv. Mater.* **2010**, *22*, 4925–4943.
3. Park, C.; Lim, J.; Yun, M.; Kim, C. Photoinduced Release of Guest Molecules by Supramolecular Transformation of Self-Assembled Aggregates Derived from Dendrons. *Angew. Chem., Int. Ed.* **2008**, *47*, 2959–2963.
4. Ochs, M.; Carregal-Romero, S.; Rejman, J.; Braeckmans, K.; De Smedt, S. C.; Parak, W. J. Light-Addressable Capsules as

Caged Compound Matrix for Controlled Triggering of Cytosolic Reactions. *Angew. Chem., Int. Ed.* **2013**, *52*, 695–699.
5. Aathimanikandan, S. V.; Savariar, E. N.; Thayumanavan, S. Temperature-Sensitive Dendritic Micelles. *J. Am. Chem. Soc.* **2005**, *127*, 14922–14929.
6. Hoare, T.; Santamaria, J.; Goya, G. F.; Irusta, S.; Lin, D.; Lau, S.; Padera, R.; Langer, R.; Kohane, D. S. A Magnetically Triggered Composite Membrane for On-Demand Drug Delivery. *Nano Lett.* **2009**, *9*, 3651–3657.
7. Hernot, S.; Klibanov, A. L. Microbubbles in Ultrasound-Triggered Drug and Gene Delivery. *Adv. Drug Delivery Rev.* **2008**, *60*, 1153–1166.
8. Geers, B.; Lentacker, I.; Cool, S.; Demeester, J.; De Smedt, S. C.; Sanders, N. N. Ultrasound Responsive Doxorubicin-Loaded Microbubbles; Towards an Easy Applicable Drug Delivery Platform. *J. Controlled Release* **2010**, *148*, e59–e60.
9. Weissleder, R. A Clearer Vision for *in Vivo* Imaging. *Nat. Biotechnol.* **2001**, *19*, 316–317.
10. Kuo, T.-R.; Hovhannisyan, V. A.; Chao, Y.-C.; Chao, S.-L.; Chiang, S.-J.; Lin, S.-J.; Dong, C.-Y.; Chen, C.-C. Multiple Release Kinetics of Targeted Drug from Gold Nanorod Embedded Polyelectrolyte Conjugates Induced by Near-Infrared Laser Irradiation. *J. Am. Chem. Soc.* **2010**, *132*, 14163–14171.
11. Carregal-Romero, S.; Ochs, M.; Rivera-Gil, P.; Ganas, C.; Pavlov, A. M.; Sukhorukov, G. B.; Parak, W. J. NIR-Light Triggered Delivery of Macromolecules into the Cytosol. *J. Controlled Release* **2012**, *159*, 120–127.
12. Yavuz, M. S.; Cheng, Y.; Chen, J.; Cobley, C. M.; Zhang, Q.; Rycenga, M.; Xie, J.; Kim, C.; Wang, L. V.; Xia, Y.; *et al.* Gold Nanocages Covered by Smart Polymers for Controlled Release with Near-Infrared Light. *Nat. Mater.* **2009**, *8*, 935–939.
13. Moon, G. D.; Choi, S. W.; Cai, X.; Li, W.; Cho, E. C.; Jeong, U.; Wang, L. V.; Xia, Y. A New Theranostic System Based on Gold Nanocages and Phase-Change Materials with Unique Features for Photoacoustic Imaging and Controlled Release. *J. Am. Chem. Soc.* **2011**, *133*, 4762–4765.
14. Chang, Y.-T.; Liao, P.-Y.; Sheu, H.-S.; Tseng, Y.-J.; Cheng, F.-Y.; Yeh, C.-S. Near-Infrared Light-Responsive Intracellular Drug and siRNA Release Using Au Nanoensembles with Oligonucleotide-Capped Silica Shell. *Adv. Mater.* **2012**, *24*, 3309–3314.
15. Qin, Z.; Bischof, J. C. Thermophysical and Biological Responses of Gold Nanoparticle Laser Heating. *Chem. Soc. Rev.* **2012**, *41*, 1191–1217.
16. Wu, G.; Mikhailovsky, A.; Khant, H. A.; Fu, C.; Chiu, W.; Zasadzinski, J. A. Remotely Triggered Liposome Release by Near-Infrared Light Absorption *via* Hollow Gold Nanoshells. *J. Am. Chem. Soc.* **2008**, *130*, 8175–8177.
17. Krpetic, Z.; Nativo, P.; See, V.; Prior, I. A.; Brust, M.; Volk, M. Inflicting Controlled Nonthermal Damage to Subcellular Structures by Laser-Activated Gold Nanoparticles. *Nano Lett.* **2010**, *10*, 4549–4554.
18. Liu, Z.; Sun, X.; Nakayama-Ratchford, N.; Dai, H. Supramolecular Chemistry on Water-Soluble Carbon Nanotubes for Drug Loading and Delivery. *ACS Nano* **2007**, *1*, 50–56.
19. Liu, Z.; Robinson, J. T.; Sun, X.; Dai, H. PEGylated Nanographene Oxide for Delivery of Water-Insoluble Cancer Drugs. *J. Am. Chem. Soc.* **2008**, *130*, 10876–10877.
20. Sherlock, S. P.; Tabakman, S. M.; Xie, L.; Dai, H. Photothermally Enhanced Drug Delivery by Ultrasmall Multifunctional FeCo/Graphitic Shell Nanocrystals. *ACS Nano* **2011**, *5*, 1505–1512.
21. Zhang, L. M.; Xia, J. G.; Zhao, Q. H.; Liu, L. W.; Zhang, Z. J. Functional Graphene Oxide as a Nanocarrier for Controlled Loading and Targeted Delivery of Mixed Anticancer Drugs. *Small* **2010**, *6*, 537–544.
22. Bao, H. Q.; Pan, Y. Z.; Ping, Y.; Sahoo, N. G.; Wu, T. F.; Li, L.; Li, J.; Gan, L. H. Chitosan-Functionalized Graphene Oxide as a Nanocarrier for Drug and Gene Delivery. *Small* **2011**, *7*, 1569–1578.
23. Robinson, J. T.; Tabakman, S. M.; Liang, Y. Y.; Wang, H. L.; Casalongue, H. S.; Vinh, D.; Dai, H. J. Ultrasmall Reduced Graphene Oxide with High Near-Infrared Absorbance for Photothermal Therapy. *J. Am. Chem. Soc.* **2011**, *133*, 6825–6831.
24. Kim, H.; Namgung, R.; Singha, K.; Oh, I. K.; Kim, W. J. Graphene Oxide-Polyethylenimine Nanoconstruct as a Gene Delivery Vector and Bioimaging Tool. *Bioconjugate Chem.* **2011**, *22*, 2558–2567.
25. Kim, H.; Kim, W. J. Photothermally Controlled Gene Delivery by Reduced Graphene Oxide–Polyethylenimine Nanocomposite. *Small* **2013**, 10.1002/smll.201202636.
26. Zhang, L. M.; Lu, Z. X.; Zhao, Q. H.; Huang, J.; Shen, H.; Zhang, Z. J. Enhanced Chemotherapy Efficacy by Sequential Delivery of siRNA and Anticancer Drugs Using PEI-Grafted Graphene Oxide. *Small* **2011**, *7*, 460–464.
27. Zhang, W.; Guo, Z. Y.; Huang, D. Q.; Liu, Z. M.; Guo, X.; Zhong, H. Q. Synergistic Effect of Chemo-Photothermal Therapy Using PEGylated Graphene Oxide. *Biomaterials* **2011**, *32*, 8555–8561.
28. Yang, K.; Zhang, S.; Zhang, G.; Sun, X.; Lee, S. T.; Liu, Z. Graphene in Mice: Ultrahigh *in Vivo* Tumor Uptake and Efficient Photothermal Therapy. *Nano Lett.* **2010**, *10*, 3318–3323.
29. Li, M.; Yang, X.; Ren, J.; Qu, K.; Qu, X. Using Graphene Oxide High Near-Infrared Absorbance for Photothermal Treatment of Alzheimer's Disease. *Adv. Mater.* **2012**, *24*, 1722–1728.
30. Tian, B.; Wang, C.; Zhang, S.; Feng, L. Z.; Liu, Z. Photothermally Enhanced Photodynamic Therapy Delivered by Nano-Graphene Oxide. *ACS Nano* **2011**, *5*, 7000–7009.
31. Sahu, A.; Choi, W. I.; Tae, G. A Stimuli-Sensitive Injectable Graphene Oxide Composite Hydrogel. *Chem Commun.* **2012**, *48*, 5820–5822.
32. Akhavan, O.; Ghaderi, E.; Aghayee, S.; Fereydooni, Y.; Talebi, A. The Use of a Glucose-Reduced Graphene Oxide Suspension for Photothermal Cancer Therapy. *J. Mater. Chem.* **2012**, *22*, 13773–13781.
33. Hu, S. H.; Chen, Y. W.; Hung, W. T.; Chen, I. W.; Chen, S. Y. Quantum-Dot-Tagged Reduced Graphene Oxide Nanocomposites for Bright Fluorescence Bioimaging and Photothermal Therapy Monitored *in Situ*. *Adv. Mater.* **2012**, *24*, 1748–1754.
34. Kiyomiya, K.-i.; Matsuo, S.; Kurebe, M. Mechanism of Specific Nuclear Transport of Adriamycin: The Mode of Nuclear Translocation of Adriamycin-Proteasome Complex. *Cancer Res.* **2001**, *61*, 2467–2471.
35. Son, S.; Namgung, R.; Kim, J.; Singha, K.; Kim, W. J. Bioreducible Polymers for Gene Silencing and Delivery. *Acc. Chem. Res.* **2011**, *45*, 1100–1112.
36. Dembereldorj, U.; Kim, M.; Kim, S.; Ganbold, E.-O.; Lee, S. Y.; Joo, S.-W. A Spatiotemporal Anticancer Drug Release Platform of PEGylated Graphene Oxide Triggered by Glutathione *in Vitro* and *in Vivo*. *J. Mater. Chem.* **2012**, *22*, 23845–23851.
37. Szabó, T.; Berkesi, O.; Forgó, P.; Josepovits, K.; Sanakis, Y.; Petridis, D.; Dékány, I. Evolution of Surface Functional Groups in a Series of Progressively Oxidized Graphite Oxides. *Chem. Mater.* **2006**, *18*, 2740–2749.
38. Moon, I. K.; Lee, J.; Ruoff, R. S.; Lee, H. Reduced Graphene Oxide by Chemical Graphitization. *Nat. Commun.* **2010**, *1*, 73–78.
39. Moon, H. K.; Lee, S. H.; Choi, H. C. *In Vivo* Near-Infrared Mediated Tumor Destruction by Photothermal Effect of Carbon Nanotubes. *ACS Nano* **2009**, *3*, 3707–3713.
40. Kim, J.; Cote, L. J.; Kim, F.; Huang, J. Visualizing Graphene Based Sheets by Fluorescence Quenching Microscopy. *J. Am. Chem. Soc.* **2009**, *132*, 260–267.
41. Yang, K.; Wan, J.; Zhang, S.; Tian, B.; Zhang, Y.; Liu, Z. The Influence of Surface Chemistry and Size of Nanoscale Graphene Oxide on Photothermal Therapy of Cancer Using Ultra-Low Laser Power. *Biomaterials* **2012**, *33*, 2206–2214.
42. Wu, M.; Kempaiah, R.; Huang, P. J.; Maheshwari, V.; Liu, J. Adsorption and Desorption of DNA on Graphene Oxide

Studied by Fluorescently Labeled Oligonucleotides. *Langmuir* **2011**, *27*, 2731–2738.
43. Zhang, R. Y.; Olin, H. Carbon Nanomaterials as Drug Carriers: Real Time Drug Release Investigation. *Mater. Sci. Eng. C* **2012**, *32*, 1247–1252.
44. Zhang, C.; Gao, S.; Jiang, W.; Lin, S.; Du, F.; Li, Z.; Huang, W. Targeted Minicircle DNA Delivery Using Folate–Poly(ethylene glycol)–Polyethylenimine as Non-Viral Carrier. *Biomaterials* **2010**, *31*, 6075–6086.
45. You, J.-O.; Auguste, D. T. The Effect of Swelling and Cationic Character on Gene Transfection by pH-Sensitive Nanocarriers. *Biomaterials* **2010**, *31*, 6859–6866.